Biomedical Signal Processing and Control 20 (2015) 125–134

Contents lists available at ScienceDirect

Biomedical Signal Processing and Control

journal homepage: www.elsevier.com/locate/bspc

Nonlocal linear minimum mean square error methods for denoising MRI

P.V. Sudeep[a,*], P. Palanisamy[a], Chandrasekharan Kesavadas[b], Jeny Rajan[c]

[a] Department of Electronics and Communication Engineering, National Institute of Technology, Tiruchirappalli, Tamil Nadu, India
[b] Department of Imaging Sciences and Intervention Radiology, Sree Chitra Tirunal Institute for Medical Sciences and Technology, Trivandrum, Kerala, India
[c] Department of Computer Science and Engineering, National Institute of Technology Karnataka, Surathkal, India

ARTICLE INFO

Article history:
Received 5 December 2014
Received in revised form 22 April 2015
Accepted 27 April 2015
Available online 16 May 2015

Keywords:
Denoising
Discrete cosine transform
Linear minimum mean square error
Magnetic resonance image
Principal component analysis
Rician distribution

ABSTRACT

The presence of noise results in quality deterioration of magnetic resonance (MR) images and thus limits the visual inspection and influence the quantitative measurements from the data. In this work, an efficient two stage linear minimum mean square error (LMMSE) method is proposed for the enhancement of magnitude MR images in which data in the presence of noise follows a Rician distribution. The conventional Rician LMMSE estimator determines a closed-form analytical solution to the aforementioned inverse problem. Even-though computationally efficient, this approach fails to take advantage of data redundancy in the 3D MR data and hence leads to a suboptimal filtering performance. Motivated by this observation, we put forward the concept of nonlocal implementation with LMMSE estimation method. To select appropriate samples for the nonlocal version of the LMMSE estimation, the similarity weights are computed using Euclidean distance between either the gray level values in the spatial domain or the coefficients in the transformed domain. Assuming that the signal dependent component of the noise is optimally suppressed by this filtering and the rest is a white and uncorrelated noise with the image, we adopt a second stage LMMSE filtering in the principal component analysis (PCA) domain to further enhance the image and the noise variance is adaptively adjusted. Experiments on both simulated and real data show that the proposed filters have excellent filtering performance over other state-of-the-art methods.

1. Introduction

Magnetic resonance imaging (MRI) is an invaluable diagnostic tool and an essential noninvasive imaging modality that provides a vast amount of anatomical and functional information useful for diagnosis and patient treatment. It is often the case that the noise in the magnitude MR images follows Rician distribution when acquired with single coil. Consideration of how noise affects the true signal is important for proper interpretation and analysis of MR images [1].

Noise filtering plays an important role in the enhancement of MR images. A plethora of different denoising methods have been proposed in last two decades [2]. Many authors directly applied traditional smoothing filters and conventional classical denoising techniques to treat the noise in MR images with an assumption of the Gaussian distributed noise model. However, those attempts have been failed to minimize the bias due to Rician noise. The bias becomes particularly important in low SNR MR images and it increases with decreasing SNR.

As a solution to the aforementioned problem, numerous methods have been proposed in the literatures that can be mainly classified into those based on partial differential equations (PDE) [3–8], wavelet based methods [9–11], nonlocal means (NLM) [12–16] or nonlocal maximum likelihood (NLMl) methods [17–21]. Wavelet-based filters are rooted in the processing of images in a transformed domain. Bao and Zhang [22] reduced the noise in MR images based on an adaptive multiscale products threshold which incorporates the merits of interscale dependencies into the thresholding technique for denoising. Other transforms that have been applied to denoise images include principal component analysis (PCA) [23] and discrete cosine transform (DCT) [24]. Many transform domain filters have derived based on the transform-threshold-inverse transform principles. An adaptive diffusion method for magnitude MR data was proposed by Sijbers et al. [4]. Also, the authors in [5] proposed a noise adaptive nonlinear diffusion technique to denoise MR images with spatially varying noise

* Corresponding author. Tel.: +91 9944589569.
E-mail address: spvnitt@gmail.com (P.V. Sudeep).

http://dx.doi.org/10.1016/j.bspc.2015.04.015
1746-8094/

levels. The limitations of the above mentioned techniques are that they usually tend to remove the useful high frequency details of the image and generate unnatural structures due to the undesirable estimations at edges.

Apart from the above discussed methods, another category of methods has been proposed for MR denoising that relied on the statistical estimation theorem. Sijbers et al. [25,26] estimated the noise variance from Rician distributed MR data and carried out signal estimation using a maximum likelihood (ML) method [19,27]. Other customized versions of the ML method have been addressed in [17,28,29]. He et al. proposed a nonlocal ML (NLML) estimation method to overcome the disadvantages of local ML method such as blurring of edges and the distortion of fine structures in the image. In that method, the samples for the ML estimation are selected in a nonlocal way based on the intensity similarity measurement of the pixel neighborhoods using the Euclidean distance. In 2014, Rajan et al. [20] presented a new NLML estimation method, for noise reduction in MR images that follows Rician distribution, in which the samples are selected in an adaptive and statistically supported way using the Kolmogorov–Smirnov test. Wong et al. [30] proposed a novel stochastic noise reduction method for MR data which utilizes Quasi-Monte Carlo estimation (QMCE) approach for estimating the noise-free signal. The QMCE approach learns the statistical characteristics of the underlying noise distribution, as well as taking into account the regional statistics of the observed signal, in a data-adaptive manner.

Recently, Aja-Fernández et al. [31,32] suggested a computationally efficient noise-driven anisotropic diffusion filtering based on a closed-form Rician LMMSE estimator for the large 3D MR images. This method estimates the noiseless signal value using local statistics of the observed image contents, i.e., by selecting a set of pixels from a local neighborhood. So, the high frequency components of the image like edges and fine details where the different underlying gray levels in a local neighborhood lead to the different realizations of its Rician nature; as a result of which, adverse estimation will be obtained. In an attempt to avoid the problem, Sudeep et al. [33] proposed a hybrid algorithm by incorporating the goodness of LMMSE estimation approach with Split-Bregman TV denoising method through 3D wavelet-subband mixing method to improve the quality of the denoised image. Since the MR data intrinsically contain many similar samples (patches) that can be used to improve the estimation results, Golshen et al. [34] addressed this difficulty by developing an SNR adapted nonlocal LMMSE method that takes the advantage of the high degree of redundancy in the contents of MR images and using a similarity measure based on the local statistical moments of the image. In [35], a filter based on nonlocal neutrosophic set (NLNS) approach was proposed. Filter bank based nonlocal means [36], iterative bilateral filtering [37], MR denoising in the wavelet packet transformed domain [38] are the other latest trends of the research area.

In this paper we proposed an improved LMMSE method for denoising magnitude MR images in which the data (in the presence of noise) follows Rician distribution. The rest of the paper is structured as follows: Section 2 presents the relevant background on the noise characteristics in MRI. Section 3 elaborates the proposed method. Section 4 deals with the experimental results, comparative evaluation and discussion, followed by the conclusions and remarks in Section 5.

2. Noise in MRI

2.1. Noise characteristics in MRI

The real and imaginary part of the raw complex valued MRI data, with mean values A_R and A_I respectively, are corrupted by white Gaussian noise with variance σ_n^2. Since the computation of magnitude image, as the root of the sum of squares (SoS) of the real and imaginary part of the complex signal, is a nonlinear operation, the distribution of the observed magnitude MR data with noise will be Rician distributed and is given by [39]:

$$p_M(M|A,\sigma_n) = \frac{M}{\sigma_n^2} e^{-(M^2+A^2/2\sigma_n^2)} I_0\left(\frac{AM}{\sigma_n^2}\right) H(M) \tag{1}$$

where I_0 is the 0th order modified Bessel function of the first kind. Here, M denotes the Rician distributed random variable, $A = \sqrt{(A_R^2 + A_I^2)}$ and $H(\cdot)$ represents the Heaviside step function. The shape of the Rician distribution depends on the signal to noise ratio (SNR), which is here defined as the ratio A/σ_n. At high SNR, i.e., when $A/\sigma_n \to \infty$, the Rician distribution approaches a Gaussian distribution and its probability density function (PDF) can be written as [39]:

$$p_M(M,\sigma_n) = \frac{1}{\sqrt{2\pi\sigma_n^2}} e^{-((M-A)^2/2\sigma_n^2)} H(M) \tag{2}$$

In the image background, where A equals zero, the Rician PDF simplifies to Rayleigh distribution [40]:

$$p_M(M,\sigma_n) = p_M(M|A=0,\sigma_n) = \frac{M}{\sigma_n^2} e^{-(M^2/2\sigma_n^2)} H(M) \tag{3}$$

2.2. Noise estimation

Although all information is contained in the real and imaginary parts of the complex data acquired by an MRI system, the usual output of the scanners are magnitude images. The straight forward and most reliable approach to estimate noise from the magnitude images is to use a double acquisition method. When two images of the same subject are acquired under identical imaging conditions, noise variance can be estimated using the averaged and single images. Many methods have been proposed in the literature to estimate the noise from magnitude MR images [41]. A survey of those methods are given in [42]. However most of the methods proposed in the literature exploit the Rayleigh distributed background region for noise estimation. These methods may not work properly when the background is very less. Recently some object based methods are proposed in literature [43,44] and these methods doesn't depends on the background for noise estimation. In this paper, we followed [44] for estimating the noise from the MR images.

3. Theory and method

3.1. Signal estimation using LMMSE estimator

The most extensively used estimator to obtain a closed-form solution for a signal that obeys a Rician PDF is the LMMSE estimator. Closed form estimation methods are more efficient with computations than optimization based solutions like maximum likelihood (ML) and expectation maximization (EM) techniques. Aja-Fernández et al. have shown that $\mathbf{A}^2$ instead of $\mathbf{A}$ can be used to achieve a closed form expression whereby all moments to be used will be even. The LMMSE estimator for Rician distributed data, that is simplified for point wise estimation, is defined as [34]:

$$\hat{A}_{i,j,k}^2 = \langle M_{i,j,k}^2 \rangle - 2\sigma_n^2 + (M_{i,j,k}^2 - \langle M_{i,j,k}^2 \rangle) \times \max\left(1 - \frac{4\sigma_n^2(\langle M_{i,j,k}^2 \rangle - \sigma_n^2)}{\langle M_{i,j,k}^4 \rangle - \langle M_{i,j,k}^2 \rangle}, 0\right) \tag{4}$$

where the notation $\langle\cdot\rangle$ is the sample estimator of the expectation, $\hat{A}_{i,j,k}$ is the estimated value of the original noiseless intensity value $A_{i,j,k}$ in the voxel (i, j, k) and $M_{i,j,k}$ the observed intensity value.

3.2. Overview of PCA domain shrinkage technique

PCA is a classical decorrelation technique that uses factorization to transform data according to its statistical properties. It has been widely used in signal processing, pattern recognition, dimensionality reduction, etc. Often the directions in which the input dataset have largest variances called principal components (PCs) are regarded as important whereas the minor components (MCs) (i.e., those components with the smallest variances) are regarded as unimportant or associated with noise. Therefore, the signal and noise can be better distinguished in the PCA domain. By transforming the original dataset into PCA domain and preserving only the PCs, the noise and trivial information can be removed [45].

In this brief presentation of the LPG-PCA technique, we closely follow [46], which the reader can refer for more details. A pixel in the noisy input image and its nearest neighbors are modeled as a m-component vector variable $\mathbf{u_v}$ and perform noise reduction on the vector instead of the single pixel in order to preserve the edges. The n training samples of $\mathbf{u_v}$ are selected by grouping the pixels with similar local spatial structures to the underlying one in the local window and forms the $m \times n$ dataset matrix $\mathbf{U_v}$.Those local statistics of the variables is accurately computed using the local pixel grouping (LPG) technique so that the image edge structures can be well preserved after shrinkage in the PCA domain for noise removal. The LPG-PCA method is a spatially adaptive image representation so that it can better characterize the image local structures.

The PCA domain shrinkage procedure is as follows: let us denote the noisy vector $\mathbf{u_v} = [u_1^v, \ldots, u_m^v]^T$ of $\mathbf{u} = [u_1, \ldots, u_m]^T$ by $\mathbf{u_v} = \mathbf{u} + \mathbf{v}$. If the dataset of noise variable $\mathbf{v} = [v_1, \ldots, v_m]^T$ is $\mathbf{V} = [V_1^T, \ldots, V_m^T]^T$ and $\mathbf{U} = [U_1^T, \ldots, U_m^T]^T$ is the decorrelated dataset of vector $\mathbf{u}$, the noise corrupted data set $\mathbf{U_v} = [(U_1^v)^T, \ldots, (U_m^v)^T]^T$ can be modeled as $\mathbf{U_v} = \mathbf{U} + \mathbf{V}$. Also, U_k denotes the row vector containing the n samples of u_k and V_k is the row sample vector of v_k. The dataset $\mathbf{U_v}$ is the sample matrix of $\mathbf{u_v}$ and its kth row, denoted as U_k^v, is the vector of $u_k^{(v)j}$s with j is varying from 1 to n.

Let the mean value of sample vector U_k^v is μ_k. Then, it can be centralized as $\bar{U}_k^v = U_k^v - \mu_k$ and the centralized matrix of $\mathbf{U_v}$ can be represented as,

$$\bar{\mathbf{U}}_\mathbf{v} = \bar{\mathbf{U}} + \mathbf{V} \tag{5}$$

Since the covariance matrix $\boldsymbol{\Omega}_{\bar{\mathbf{U}}}$ of the centralized dataset $\bar{\mathbf{U}}$ is symmetrical, it can be decomposed as $\boldsymbol{\Omega}_{\bar{\mathbf{U}}} = \boldsymbol{\Phi}_{\bar{\mathbf{U}}} \boldsymbol{\Lambda}_{\bar{\mathbf{U}}} \boldsymbol{\Phi}_{\bar{\mathbf{U}}}^T$, where $\boldsymbol{\Phi}_{\bar{\mathbf{U}}}$ is the orthonormal eigenvector matrix and $\boldsymbol{\Lambda}_{\bar{\mathbf{U}}}$ is the diagonal eigen value matrix of $\boldsymbol{\Omega}_{\bar{\mathbf{U}}}$ respectively.

In practical implementation, we can set the orthonormal transformation matrix $\mathbf{P}_{\bar{\mathbf{U}}} = \boldsymbol{\Phi}_{\bar{\mathbf{U}}}^T$ to decorrelate $\bar{\mathbf{U}}_\mathbf{v}$ i.e., $\bar{\mathbf{S}}_\mathbf{v} = \mathbf{P}_{\bar{\mathbf{U}}} \bar{\mathbf{U}}_\mathbf{v}$. The covariance matrix of noisy dataset $\boldsymbol{\Omega}_{\bar{\mathbf{S}}_\mathbf{v}}$ can be represented in terms of covariance matrix of decorrelated dataset $\boldsymbol{\Omega}_{\bar{\mathbf{S}}}$ and the covariance matrix of the noise dataset $\boldsymbol{\Omega}_{\mathbf{v_s}}$ as [46]

$$\boldsymbol{\Omega}_{\bar{\mathbf{S}}_\mathbf{v}} = \boldsymbol{\Omega}_{\bar{\mathbf{S}}} + \boldsymbol{\Omega}_{\mathbf{v_s}} \tag{6}$$

In the PCA transformed domain, the noise in $\bar{\mathbf{S}}_\mathbf{v}$ is suppressed by using the LMMSE technique. The LMMSE of kth row of $\bar{\mathbf{S}}$, denoted as $\bar{\bar{S}}_k$, can be achieved through the multiplication of the $\bar{\mathbf{S}}_\mathbf{v}$ (i.e., $\bar{\bar{S}}_v^k$) with the shrinkage coefficient w_k. i.e.,

$$\hat{\bar{\bar{S}}}_v^k = w_k \cdot \bar{\bar{S}}_v^k \tag{7}$$

where $w_k = \boldsymbol{\Omega}_{\bar{\mathbf{S}}}(k,k)/(\boldsymbol{\Omega}_{\bar{\mathbf{S}}}(k,k) + \boldsymbol{\Omega}_{\mathbf{v_s}}(k,k))$

Assume the matrix $\hat{\bar{\mathbf{S}}}$ contains all $\hat{\bar{\bar{S}}}_v^k$. Then, we can find the denoised result $\hat{\bar{\mathbf{U}}}$ of $\bar{\mathbf{U}}_\mathbf{v}$ as,

$$\hat{\bar{\mathbf{U}}} = \mathbf{P}_{\bar{\mathbf{U}}}^T \hat{\bar{\mathbf{S}}} \tag{8}$$

Adding the mean values μ_k back to $\hat{\bar{\mathbf{U}}}$ gives the denoised dataset $\hat{\mathbf{U}}$. Applying the above procedure to all the pixels leads to the full denoised image of the noisy image.

3.3. Proposed approach

The non-local principle exploits the fact that similar neighborhoods can occur anywhere in the image and is able to yield high-quality denoising results. So, the nonlocal version of LMMSE (NLLMMSE) estimation for Rician noise model is proposed in this paper for MR denoising. In this non-local method, the center voxel of two similar volumes in the magnitude MR data have a similar meaning for the image and thus similar gray values. They can be understood as two noisy measurements of the same noise-free patch.

The common way for the measurement of similarity is by using the Euclidean distance between the two vectors formed by the neighborhood voxels in the similarity volume of the voxel i and j (i.e., in the spatial domain). Let $(A_i)_p$ and $(A_j)_p$ be the pth elements in the vectors $\mathbf{A}_i$ and $\mathbf{A}_j$ respectively. Then, the Euclidean distance is defined as,

$$\|\mathbf{A}_i - \mathbf{A}_j\|^2 = \sum_{p=1}^{P} ((A_i)_p - (A_j)_p)^2 \tag{9}$$

Algorithm for NLLMMSE filter to denoise the Rician affected noisy image is provided in Algorithm 1.

It was shown that the noise in MR images can adversely affect the selection of samples with similar underlying gray value and a restricted local ML (RLML) estimation method has been presented in [19] by creating a reference image using NLM method to address it. More recently, calculation of similarity weights in DCT subspace were proposed for improving the performance of 2D NLM filter [47]. This DCT based NLM filter computes the similarity accurately and with less computational burden.

We can extend this concept of similarity weight calculation in DCT domain with 2D NLLMMSE Filter to get 2D NLLMMSE-DCT Filter. Since the availability of appropriate samples for LMMSE estimation is higher in the near neighborhood of 3D MR data points and hence an explicitly better performance for 3D filtering over 2D filtering, we have preferred to work with 3D NLLMMSE-DCT Filter and is summarized as in Algorithm 2. Notice that, the above mentioned 3D NLLMMSE-DCT filter have chosen the parameters such as search volume size, similarity volume size and the number of DCT coefficients to find the distance measure as same as that of NLLMMSE filter to ensure a similar experimental setup for both the filters. We can further improve the performance of 3D NLLMSE-DCT filter by selecting a very large search volume and a lesser DCT subspace.

The DCT transform for 3D data can be defined as,

$$Cd_i = C_{l,m,n}^{(i)} \tag{10}$$

$$Cd_i = \alpha(l)\alpha(m)\alpha(n) \sum_{x=0}^{r-1} \sum_{y=0}^{r-1} \sum_{z=0}^{r-1} A_i \cos\left[\frac{\pi(2x+1)l}{2r}\right] \times \cos\left[\frac{\pi(2y+1)m}{2r}\right] \cos\left[\frac{\pi(2z+1)n}{2r}\right],$$

$$l, m, n = 0, 1, \ldots, r-1$$

where Cd_i represents the coefficients in DCT subspace of A_i, r is the length, breadth or height of A_i and $\alpha(\star)$, $\star = l, m, n$ is defined as,

$$\alpha(\star) = \begin{cases} \sqrt{\frac{1}{r}} & \text{for} \star = 0, \\ \sqrt{\frac{1}{2r}} & \text{for} \star \neq 0. \end{cases} \tag{11}$$

in the first dimension and followed by second and third dimensions. Notice that this way of 3D DCT computation will increase time complexity tremendously. Hence, we used a much faster multi-dimensional DCT implementation of Andriy Myronenko [48] which utilizes the advantage of Fast Fourier Transform (FFT), fast permutation through indices and persistent pre-computation.

In order to obtain the DCT coefficient vector for the similarity check, we convert the input volume of size $r \times r \times r$ around each voxel into the DCT volume of similar size [48]. Here, we fixed the value of $r = 3$ to achieve better computational efficiency. The first element in the (1,1,1) position of the DCT coefficient matrix is the DC coefficient and most of the energy will be compacted in this coefficient. The second layer of the DCT volume, i.e., the $2 \times 2 \times 2$ block except the DC coefficient, corresponds to the mid-frequency range signal and the rest of the coefficients correspond to the high frequency layer. In case of NLLMMSE-DCT filter, each of these sub-bands of two DCT volumes are compared in terms of the distance $\| Cd(N_i) - Cd(N_j) \|^2$, i.e., the samples are selected by comparing the energy in each subband of the DCT volumes. Those volumes having smaller value for the difference in sub-band energies will produce a small value (approximately zero) for the similarity measure. The results in the following sections will validate the effectiveness of this method.

Most of the initial noise will be removed in the first stage of the algorithm and its output $\hat{\mathbf{F}} = NLLMMSE[\mathbf{G}]$ is an image with good PSNR. Even though the quality is much improved, there is still visually unpleasant noise residual in the denoised image $\hat{\mathbf{F}}$. Although once the image $\mathbf{G}$ is filtered with the Rician estimator in nonlocal way, the output model is no longer Rician. Hence, applying the recursive version of the filter can not handle the noise effectively. One another consequence of this recursive approach is the unnecessary computational burden. In order to reduce this noise residual, $\hat{\mathbf{F}}$ can be applied to the LPG-PCA denoising procedure[46] with adaptively adjusted noise standard deviation.

The underlying assumption for second stage filtering is that the first stage removes the signal dependent component (Rician) of the noise in the image effectively and the rest of it in $\hat{\mathbf{F}}$ can be treated as a white Gaussian noise. The LPG-PCA filter is a good choice to remove such noises in images. But, it is important that the noise level must update to work the LPG-PCA filter properly. The noise standard deviation estimate $\hat{\sigma_s}$ of second stage can be calculated from the local variance distribution as [31],

$$\hat{\sigma_s^2} = \text{mode}\{\sigma_{N_i}^2\} \tag{12}$$

where $\sigma_{N_i}^2$ represents the local variance distribution obtained by using the neighborhood N_i around each pixel i. We used the neighborhood window of size 7×7.

Algorithm 1. Signal estimation using NLLMMSE filter

Input: $\mathbf{G} \Leftarrow$ Noisy MR Data
Noise standard deviation estimation: Find standard deviation σ_n from $\mathbf{G}$ [followed the method in [44]]
for each voxel $g(i)$ of $\mathbf{G}$ **do**
  Select a $R \times R \times R$ *SearchVolume* around the voxel
  $N_i \Leftarrow$ Similarity volume of size $r \times r \times r$ around the voxel
  $N_j, j = 1 \cdots (R^3 - 1) \Leftarrow$ Neighbourhood volumes in the *SearchVolume* other than N_i
  Compute the distance $\left\| g(N_i) - g(N_j) \right\|^2$ and create a list D
  $O = sort(D)$ i.e., rank D in ascending order.
  Choose the first l elements of O for applying next step.
  Compute $\hat{f}_i^2 \leftarrow$ LMMSE estimation of the samples using (4).
  Find $\hat{f}_i \leftarrow$ square root of $\hat{f}_i^2$
end for
Output: $\hat{\mathbf{F}} \Leftarrow$ Denoised MR Data

Algorithm 2. Signal estimation using NLLMMSE-DCT Filter

Input: $\mathbf{G} \Leftarrow$ Noisy MR Data
Noise standard deviation estimation: Find standard deviation σ_n from $\mathbf{G}$ [followed the method in [44]]
for each voxel $g(i)$ of $\mathbf{G}$ **do**
  Select a $R \times R \times R$ *SearchVolume* around the voxel
  $N_i \Leftarrow$ Similarity volume of size $r \times r \times r$ around the voxel
  $N_j, j = 1 \cdots (R^3 - 1) \Leftarrow$ Neighbourhood volumes in the *SearchVolume* other than N_i
  Transform N_i and N_js using 3D-DCT as in (10) to obtain $Cd(N_i)$ and $Cd(N_j)$s respectively.
  Compute the distance $\left\| Cd(N_i) - Cd(N_j) \right\|^2$ and create a list D
  $O = sort(D)$ i.e., rank D in ascending order.
  Choose the first l elements of O for applying next step.
  Compute $\hat{f}_i^2 \leftarrow$ LMMSE estimation of the samples using (4).
  Find $\hat{f}_i \leftarrow$ square root of $\hat{f}_i^2$
end for
Output: $\hat{\mathbf{F}} \Leftarrow$ Denoised MR Data

Consider a central block of size $K \times K$ and a training block of size $L \times L$, where $K < L$, around a pixel to be denoised. Let u_0^v be the column sample vector containing the central $K \times K$ block and u_i^v, $i = 1, 2, \ldots, \kappa$ and $\kappa = (L - K + 1)^2 - 1$ of length K^2 be the sample vectors corresponding to the other blocks in the training window. Since the training window contains very different blocks from the given central block, usage of all the $K \times K$ blocks as the training samples of $\mathbf{u_v} = [u_1^v, \ldots, u_i^v, \ldots, u_{K^2}^v]^T$ will be directed to an inaccurate estimation of the PCA transformation matrix and deteriorates the quality of denoised output. To guarantee an efficient selection of training samples and the accuracy of the results, the LPG mechanism is implemented as in Eq. (13).

$$E_i = \frac{1}{K^2} \sum_{k=1}^{K^2} (u_0^v(k) - u_i^v(k))^2 \tag{13}$$

For a preset value of γ, we will check whether $E_i < \gamma + 2\hat{\sigma_s^2}$. All the u_i^v's that satisfies this criteria including the central vector u_0^v form the sample vector of $\mathbf{u_v}$, i.e., the training data set $\mathbf{U_v}$. In practice, we will use at least $n = c \cdot K^2$ training samples of $\mathbf{u_v}$ in denoising, where c is a constant, to ensure the number of samples to find the PCA transformation matrix $\mathbf{P_{\tilde{U}}}$. The top n samples are robust to estimate the image local statistics, and this operation makes the algorithm more stable to calculate $\mathbf{P_{\tilde{U}}}$.

The methodology as summarized below:

1 In case of real MRI, the noise level in the input image is unknown. So, estimation of noise standard deviation in the image is a prior requirement and can be achieved through the technique discussed in [44].
2 In the first stage, an effective noise removal is attained through the nonlocal implementation of LMMSE estimator for Rician noise using Euclidean distance as the measure for blocks comparison. It can be performed either in spatial domain (in case

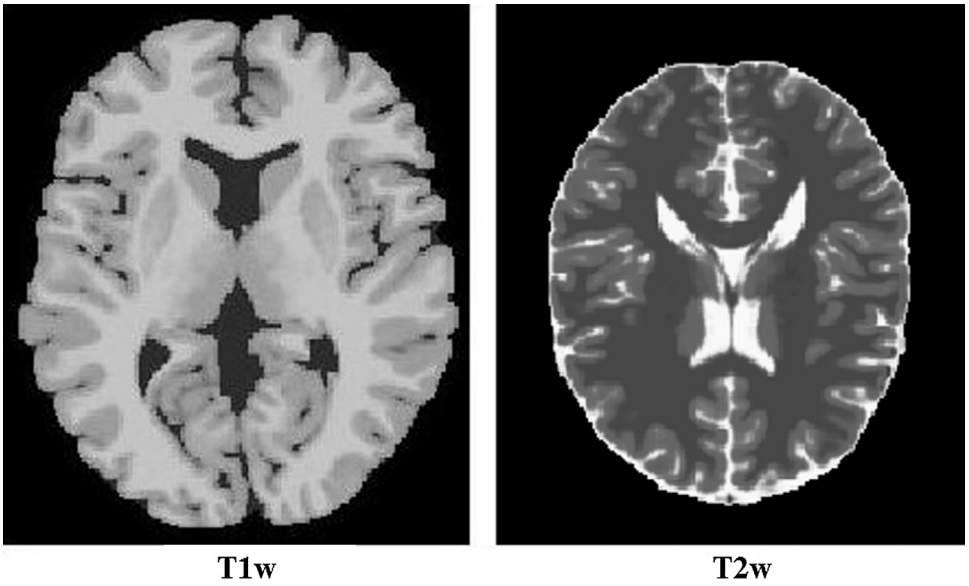

Fig. 1. Simulated MR images used for the experiment: original T1w, T2w images from the BrainWeb Database.

Table 1
Comparison of results based on PSNR.

Method	PSNR							
	$\sigma = 5$	$\sigma = 10$	$\sigma = 15$	$\sigma = 20$	$\sigma = 25$	$\sigma = 30$	$\sigma = 35$	$\sigma = 40$
Noisy	35.7466	29.7135	26.2144	23.7541	21.9016	20.2565	18.9671	17.7789
UNLM	40.0682	35.9584	32.8175	30.8298	29.3857	27.9769	27.3820	26.2652
LPG-PCA	39.6340	34.8450	32.0306	30.1946	28.7745	27.1348	26.3585	24.9334
LMMSE	38.2319	33.9380	31.7351	30.0419	28.9346	27.7401	27.0905	26.1110
NLLMMSE	40.4005	35.9696	33.0638	30.9814	29.4659	27.8618	26.7962	25.5443
NLLMMSE+LPG-PCA	**41.3806**	36.9566	34.1421	32.2871	30.8391	29.4764	28.6867	27.6557
NLLMMSE-DCT	40.5417	36.3399	33.5931	31.7318	30.4230	29.0538	28.0823	26.9783
NLLMMSE-DCT+LPG-PCA	41.0690	**37.0018**	**34.2165**	**32.5109**	**31.1776**	**29.9130**	**29.0534**	**28.1059**

Table 2
Comparison of results based on mean SSIM.

Method	Mean SSIM							
	$\sigma = 5$	$\sigma = 10$	$\sigma = 15$	$\sigma = 20$	$\sigma = 25$	$\sigma = 30$	$\sigma = 35$	$\sigma = 40$
Noisy	0.8773	0.7682	0.6791	0.6134	0.5601	0.5141	0.4771	0.4420
UNLM	0.9528	0.9145	0.8807	0.8408	0.8017	0.7567	0.7299	0.6929
LPG-PCA	0.9478	0.9045	0.8794	0.8433	0.8075	0.7733	0.7409	0.7075
LMMSE	0.9521	0.8912	0.8579	0.8179	0.7890	0.7533	0.7331	0.7109
NLLMMSE	0.9500	0.9053	0.8591	0.8121	0.7681	0.7242	0.6833	0.6451
NLLMMSE+LPG-PCA	**0.9725**	0.9435	0.9190	0.8898	0.8593	0.8285	0.7938	0.7655
NLLMMSE-DCT	0.9579	0.9221	0.8872	0.8495	0.8186	0.7846	0.7515	0.7200
NLLMMSE-DCT+LPG-PCA	0.9720	**0.9513**	**0.9268**	**0.9004**	**0.8788**	**0.8532**	**0.8246**	**0.8075**

Table 3
Comparison of results in BC.

Method	BC							
	$\sigma = 5$	$\sigma = 10$	$\sigma = 15$	$\sigma = 20$	$\sigma = 25$	$\sigma = 30$	$\sigma = 35$	$\sigma = 40$
Noisy	0.8881	0.8590	0.8391	0.8245	0.8068	0.7957	0.7827	0.7709
UNLM	0.9423	0.9251	0.9088	0.9039	0.8917	0.8821	0.8802	0.8772
LPG-PCA	0.9267	0.9096	0.9008	0.8874	0.8787	0.8592	0.8633	0.8672
LMMSE	0.9306	0.9098	0.8936	0.8836	0.8776	0.8669	0.8622	0.8566
NLLMMSE	0.9364	0.9101	0.8914	0.8810	0.8723	0.8629	0.8597	0.8524
NLLMMSE+LPG-PCA	0.9443	0.9374	0.9226	0.9142	0.9037	0.8953	0.8889	0.8927
NLLMMSE-DCT	0.9434	0.9201	0.9041	0.8934	0.8857	0.8793	0.8706	0.8661
NLLMMSE-DCT+LPG-PCA	**0.9479**	**0.9461**	**0.9289**	**0.9170**	**0.9048**	**0.9006**	**0.8954**	**0.8956**

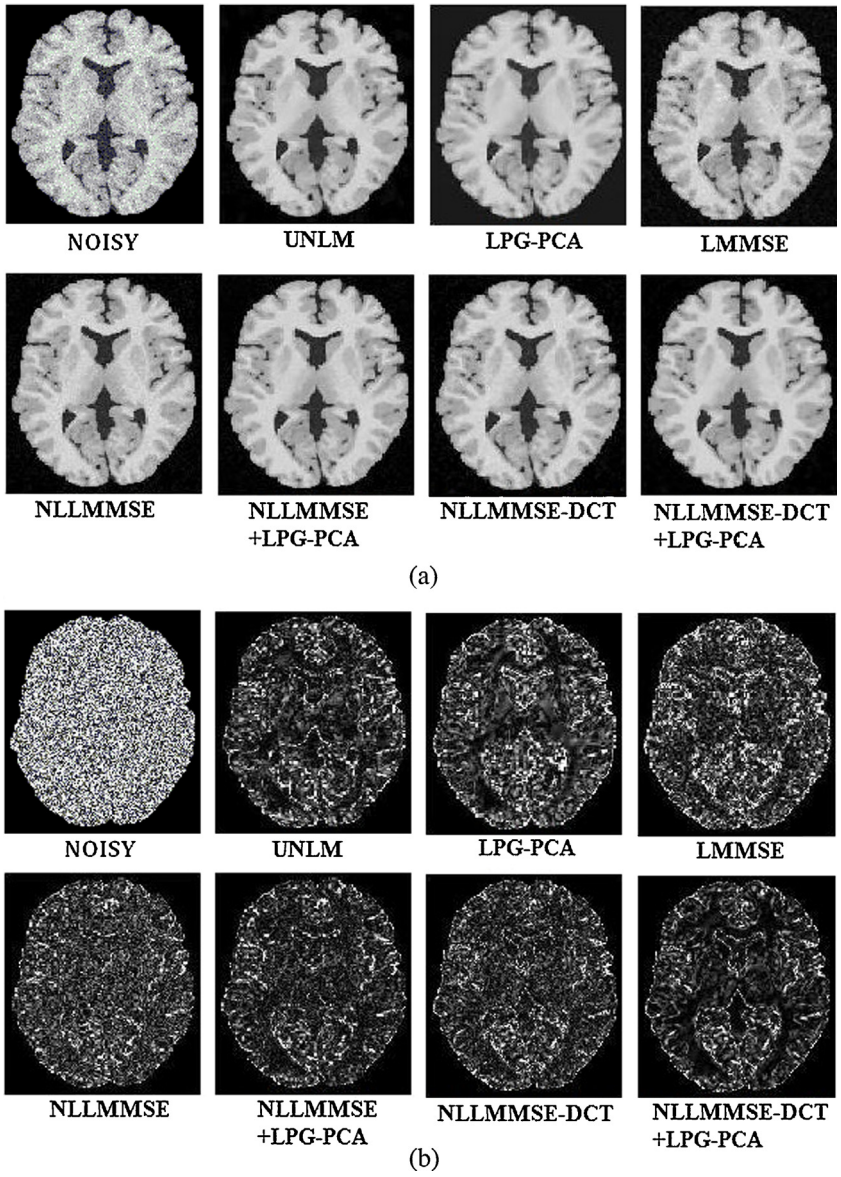

Fig. 2. Qualitative comparison of experimental results on the synthetic T1w MR volume (Rician noise of $\sigma_n = 20$). (a) Denoised image and (b) residuals image (in the range of [0, 25]).

of NLLMMSE filter) or in the transformed domain (in case of NLLMMSE-DCT filter).

3 The rest of the noise in the denoised image obtained from the first stage is assumed as a white and uncorrelated one with signal. The noise standard deviation of the result image is updating by using (12).
4 Local pixel grouping (LPG) in the PCA domain is used for selecting and grouping the training sample blocks with similar content to the central block.
5 After the LPG block matching, the LMMSE based shrinkage is applied to the coefficients in the PCA domain for the removal of noise in the image.
6 As the last step, the inverse PCA (IPCA) transformation is performed to obtain the final denoised image.

4. Experiments and results

In this section, we report the experimental results on synthetic datasets generated by the BrainWeb [49] simulator, real MR image of a kiwi fruit and real clinical brain MR images.

The parameters used for the various filters in this article are given below:

1 LMMSE [31] method: the LMMSE estimator used a fixed filter size of $3 \times 3 \times 3$.
2 Unbiased NLM (UNLM) [50]: The UNLM filter used a search window of size 11×11 and similarity window of size 5×5.
3 Two stage Local Pixel Grouping PCA (LPG-PCA) denoising: the LPG-PCA uses the size of the variable block as $K = 5$ and the size of training block $L = 41$. The threshold γ in the LPG grouping is set to 25.
4 NLLMMSE filter or NLLMMSE-DCT filter: The search window size is $11 \times 11 \times 3$ and similarity window has a size of $3 \times 3 \times 3$ for each voxel under processing. The number of samples (l) used for the LMMSE estimation is fixed as 100 for all values of σ_n.
5 $NLLMMSE + LPG - PCA$ filter/$NLLMMSE - DCT + LPG - PCA$ filter: the default parameters for the NLLMMSE or NLLMMSE-DCT filtering stage are used as in step 4. The second stage filter, i.e.,

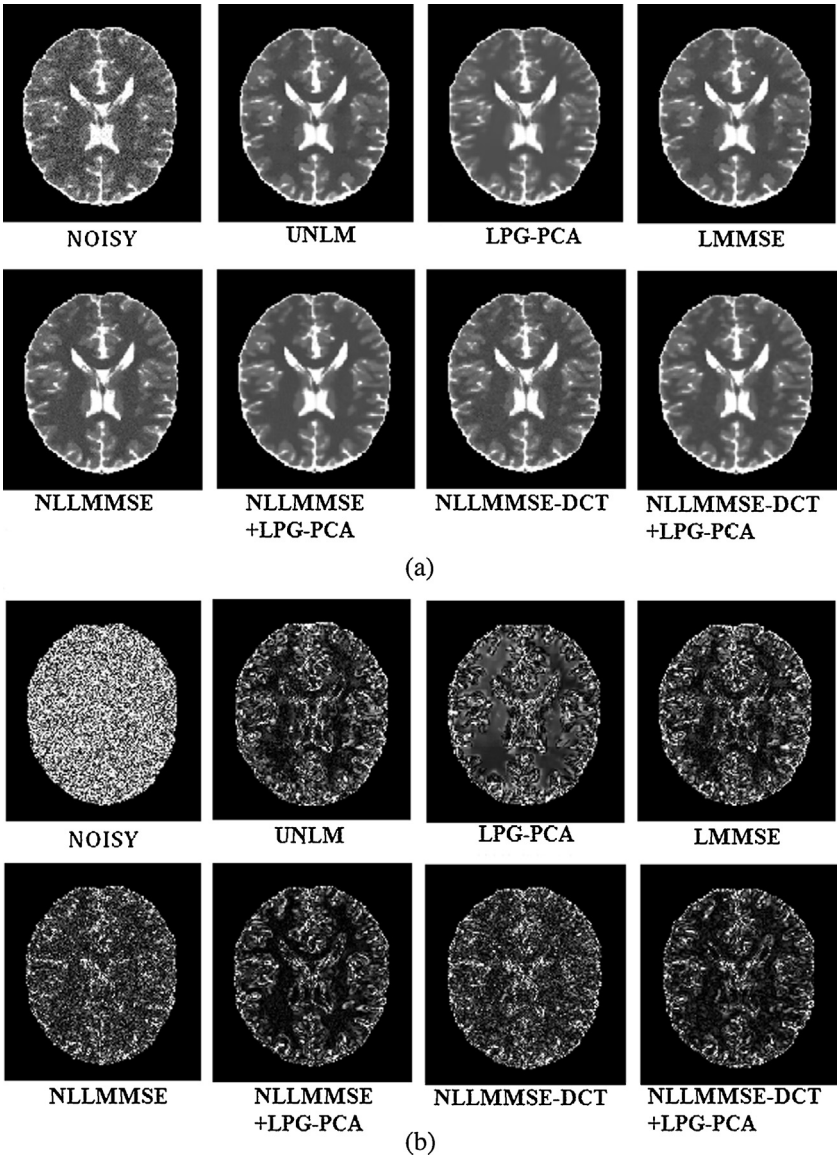

Fig. 3. Qualitative comparison of experimental results on the synthetic T2w MR volume (Rician noise of $\sigma_n = 20$). (a) Denoised image and (b) residuals image (in the range of [0, 25]).

LPG-PCA filter, used the size of the variable block as $K = 5$ and the size of training block as $L = 41$.

4.1. Visual quality comparison with synthetic images

Fig. 1 shows the slices of the synthetic test images used in our experiments. We have used T1-weighted(T1w) and T2w volumes of $181 \times 217 \times 181$ voxels with 1 mm^3 voxel resolution (intensity values in the range [0, 255]).

It is clear from the denoised results in Figs. 2 and 3 that the two stage filtering achieves much closer result to the original image than the image filtered with other proposed techniques such as NLLMSE filter and NLLMMSE-DCT filter. Qualitatively, the proposed NLLMMSE-DCT+LPG-PCA filter provides better preservation of fine structures, good contrast between tissues and fewer oscillations over homogeneous areas and better noise removal over the other methods under considerations. Notice that the residual images validate that the LPG-PCA filter acts well as the refinement stage in two stage filtering method and contributes significantly in the noise removal as well as in the image structure preservation.

4.2. Validation on real MR data

In order to test the proposed filters over real data, we carry out experiments using real 2D MR data of a kiwifruit and clinical 2D MR data set.

In the experiment discussed in Fig. 4, we applied various Rician noise model based filtering algorithms on MR image of a kiwi fruit of size 227×206 with estimated noise standard deviation $\sigma_n = 27.5$. The visual results are much better for our proposed methods in terms of image contrast. The NLLMMSE-DCT+LPG-PCA filtering method particularly performs well and removes the noise successfully.

The first columns of Figs. 5 and 6 display a typical axial cut of size 512×360 with $\sigma_n = 27$ and the sagittal cut of the real brain T1w image of size 512×512 with $\sigma_n = 15$ respectively. For a better visual comparison, we presented the results of proposed filters on a zoomed region of the image portion marked by a red rectangular box in the upper left hand images. It can be observed from these images that most of the noise have been suppressed without blurring the edges or by preserving the useful high frequency details of the image.

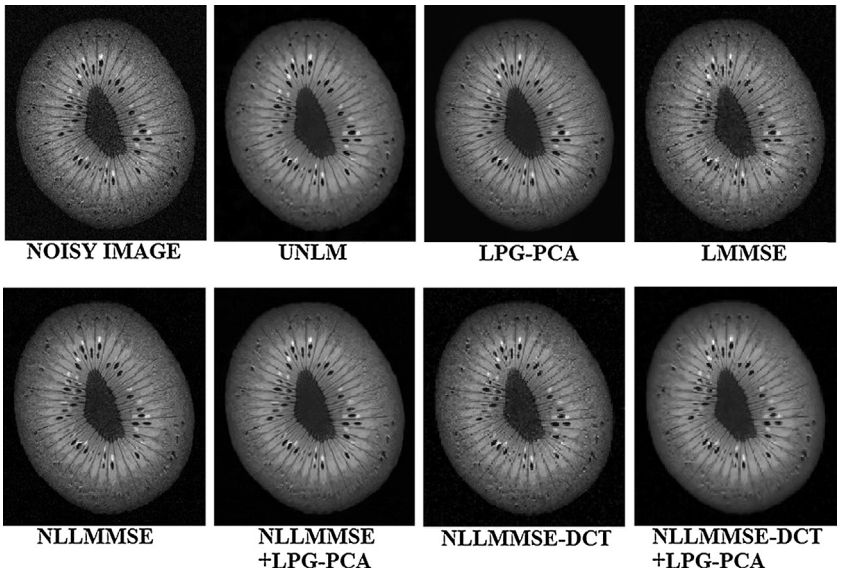

Fig. 4. Experiments on the real MR image of a kiwi fruit.

4.3. Quantitative analysis

The synthetic images were artificially corrupted with Rician noise generated for a range of noise standard deviations and the denoising efficiency of the algorithm were evaluated quantitatively. Our quantitative evaluation relies on the objective measures such as peak signal to noise ratio (PSNR)[51], mean structural similarity index matrix (SSIM) [52] and Bhattacharya coefficient (BC)[53]. The PSNR is the simplest and most widely used image quality measure evaluated in decibels (dB) and is inversely proportional to the mean squared error (MSE) after denoising. Nevertheless, it is too rough a measure of similarity because it does not account for the similarity between image structures; only for the similarity between gray levels. Hence, we used another quality measure called Mean SSIM that is more consistent with the human visual system. The Mean SSIM takes into account the similarity of the edges (high frequency content) between the denoised image and the ideal one. The BC is a measure of divergence and is used in this paper to determine the relative closeness of the two samples being considered.

To avoid any bias due to background, these three quality measures are only applied to those areas other than background. For the quantitative analysis, a repeated experiment with various values of σ_n varying from 5 to 40 has been performed. All the experiments described in this section are conducted in T1w MR data shown in Fig. 1.

In Table 1, we can observe that the NLLMMSE based methods shows a better performance over the state of the art methods like

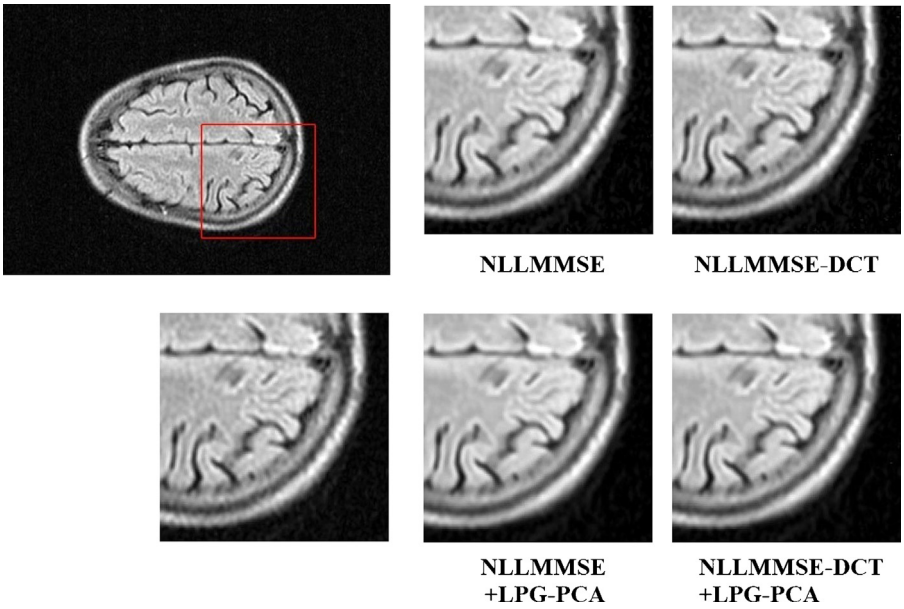

Fig. 5. Denoising results of the proposed methods on a typical axial slice of the real brain T1w MR images. First column top row shows the original image with $\sigma_n = 27$ and the magnification of the red rectangular region in the bottom. Second column from top to bottom shows the NLLMMSE and NLLMMSE+LPG-PCA filtered results corresponding to the magnified rectangular region of the noisy MR image respectively. The third column from top to bottom shows the denoising results of NLLMMSE-DCT and NLLMMSE-DCT+LPG-PCA filters. (For interpretation of the references to color in this figure legend, the reader is referred to the web version of this article.)

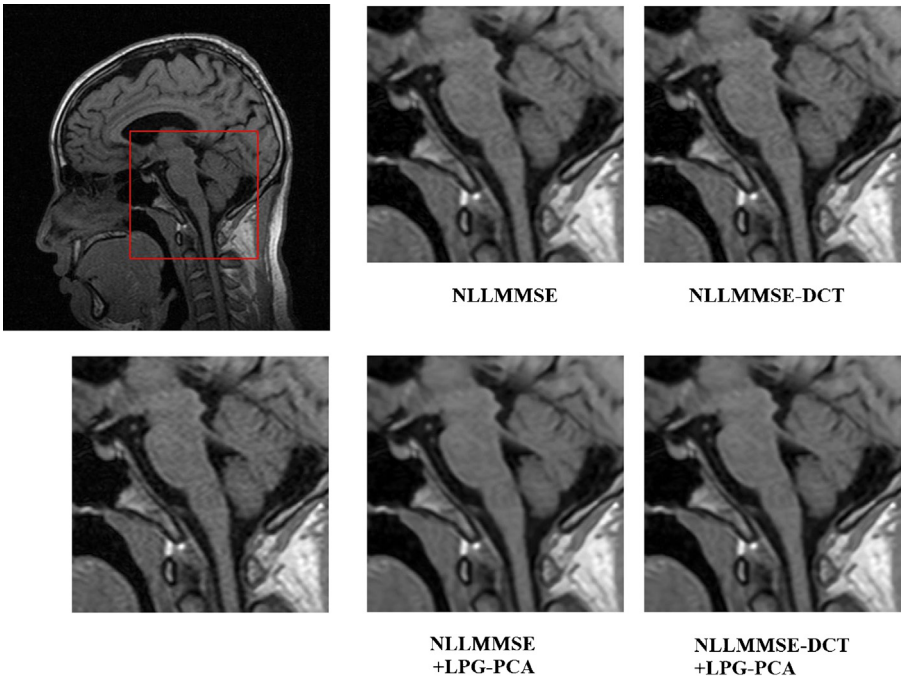

Fig. 6. Denoising results of the proposed methods on a typical sagittal slice of the real brain T1w MR images. First column top row shows the original image with $\sigma_n = 15$ and the magnification of the red rectangular region in the bottom. Second column from top to bottom shows the NLLMMSE and NLLMMSE+LPG-PCA filtered results corresponding to the magnified rectangular region of the noisy MR image respectively. The third column from top to bottom shows the denoising results of NLLMMSE-DCT and NLLMMSE-DCT+LPG-PCA filters. (For interpretation of the references to color in this figure legend, the reader is referred to the web version of this article.)

UNLM, LPG-PCA and LMMSE based on the objective measure PSNR. It should be noted that the NLLMMSE filter, that estimates the true intensity with samples obtained through a similarity calculation in the spatial domain, did not produce noticeable improvement in PSNR than the conventional LMMSE filter at high noise standard deviation. This problem is addressed in the NLLMMSE-DCT filter by selecting samples through a similarity measurement in the transformed domain using DCT. With the LPG-PCA refinement stage, the NLLMMSE-DCT+LPG-PCA filter gives the best result among the four proposed filters.

To study the behavior of the NLLMMSE-DCT filter in relation with parameters like number of coefficients for similarity calculation, size of similarity volume and search volume size, a new experiment is carried out by fixing the noise standard deviation at $\sigma_n = 20$. The PSNR value for NLLMMSE-DCT filter with DC coefficient only gives a PSNR value of 31.5787 dB and the complete transformed matrix gives a PSNR value of 31.7318 dB. Experiments also showed that variation in the size of similarity volume can affect the denoising performance. The PSNR value of the NLLMMSE-DCT filter for a similarity volume of size $3 \times 3 \times 3$ is 31.7318 dB and 30.7921 dB for a similarity volume of size $5 \times 5 \times 5$. The result of experiments on T1w MR Data by varying the search volume size indicates that a larger search volume can improve the denoising performance, i.e., for a search volume of size $11 \times 11 \times 11$ gives a PSNR of 31.7318 dB, which is higher than that of a search volume size of $7 \times 7 \times 7$ (i.e., 31.2274 dB).

We compared filters such as UNLM, LMMSE, LPG-PCA and NLLMMSE based filters in terms of variation in Mean SSIM values at different noise standard deviation ranging from 5 to 40 as shown in Table 2. The range of the MSSIM value is [0, 1] and it approaches 1 when the denoised image $\hat{\mathbf{A}}$ moves closer to original image $\mathbf{A}$. Because of its relevance to the image contrast, we also used the Bhattacharya coefficient to compare the methods quantitatively as shown in Table 3.

5. Conclusion

In this paper, four filtering methods have been proposed to remove noise from the Rician distributed MR data. All these filters used the nonlocal version of the LMMSE filtering to achieve a significant quality improvement in the MR image in terms of PSNR, Mean SSIM and BC. The NLLMMSE filter with sample selection in the spatial domain has a better performance than the state of art methods such as UNLM and LMMSE filters at low SNRs. The NLLMMSE-DCT filter finds the best samples for LMMSE estimation from the DCT domain and performs well at all SNRs. The LPG-PCA filter refines and further improves the quality of the output of NLLMMSE filter as well as NLLMMSE-DCT filter. The performance of the proposed methods are well demonstrated by experiments on both simulated and real MR data.

References

[1] B.A. Landman, P.L. Bazin, J.L. Prince, Estimation and application of spatially variable noise fields in diffusion tensor imaging, Magn. Reson. Imaging 27 (July (6)) (2009) 741–751.
[2] A. Buades, B. Coll, J.M. Morel, A review of image denoising algorithms with a new one, SIAM Multiscale Model Simul. 4 (July (2)) (2005) 490–530.
[3] P. Perona, J. Malik, Scale space and edge detection using anisotropic diffusion, IEEE Trans. Pattern Anal. Mach. Intel. 12 (July (7)) (1990) 629–639.
[4] J. Sijbers, A.J. Dekker, A.V. Linden, M. Verhoye, T.M. Van Dyck, Adaptive anisotropic noise filtering for magnitude MR data, J. Magn. Reson. Imaging 17 (December (10)) (1999) 1533–1539.
[5] A.A. Samsonov, C.R. Johnson, Noise adaptive nonlinear diffusion of MR images with spatially varying noise levels, Magn. Reson. Med. 52 (October (4)) (2004) 798–806.
[6] M. Lysaker, A. Lundervold, X.C. Tai, Noise removal using fourth-order partial differential equation with applications to medical magnetic resonance images in space and time, IEEE Trans. Image Process. 12 (December (12)) (2003) 1579–1590.
[7] K. Krissian, S. Aja-Fernandez, Noise-driven anisotropic diffusion filtering of MRI, IEEE Trans. Image Process. 18 (October (10)) (2009) 2265–2274.
[8] G. Gerig, O. Kubler, R. Kikinis, F.A. Jolesz, Nonlinear anisotropic filtering of MRI data, IEEE Trans. Med. Imaging 11 (June (2)) (1992) 221–232.

[9] R.D. Nowak, Wavelet based Rician noise removal for magnetic resonance imaging, IEEE Trans. Image Process. 8 (October (10)) (1999) 1408–1419.
[10] A. Pizurica, W. Philips, I. Lemahieu, M. Acheroy, A versatile Wavelet domain noise filtration technique for medical imaging, IEEE Trans. Med. Imaging 22 (March (3)) (2003) 323–331.
[11] J.C. Wood, K.M. Johnson, Wavelet packet denoising of magnetic resonance images: importance of Rician noise at low SNR, Magn. Res. Med. 41 (March) (1999) 631–635.
[12] J.V. Manjón, J. Carbonell-Caballero, J.J. Lull, G. Garcia-Martí, L. Martí-Bonmatí, M. Robles, MRI denoising using non-local means, Med. Image Anal. 4 (August (12)) (2008) 514–523.
[13] N. Wiest-Daessle, S. Prima, P. Coupé, S. Morrissey, C. Barillot, Rician noise removal by non-local means filtering for low signal-to-noise ratio MRI: applications to DT-MRI, MICCAI 11 (2) (2008) 171–179.
[14] P. Coupé, P. Yger, S. Prima, P. Hellier, C. Kervrann, C. Barillot, An optimized blockwise nonlocal means denoising filter for 3D magnetic resonance images, IEEE Trans. Med. Imaging 27 (April (4)) (2008) 425–441.
[15] P. Coupé, P. Hellier, S. Prima, C. Kervrann, C. Barillot, 3D wavelet subbands mixing for image denoising, J. Biomed. Imaging 2008 (January (3)) (2008) 1–118.
[16] S. Duli, A. Kuurstra, I.C.S. Patarroyo, O.V. Michailovich, A new similarity measure for non-local means filtering of MRI images, J. Visual Comm. Imaging Represent. 24 (October (7)) (2013) 1040–1054.
[17] L. He, I.R. Greenshields, A nonlocal maximum likelihood estimation method for Rician noise reduction in MR images, IEEE Trans. Med. Imaging 28 (February (2)) (2009) 165–172.
[18] J. Rajan, J. Veraart, J.V. Audekerke, M. Verhoye, J. Sijbers, Nonlocal maximum likelihood estimation method for denoising multiple-coil magnetic resonance images, Magn. Reson. Imaging 30 (December (10)) (2012) 1512–1518.
[19] J. Rajan, B. Jeurissen, M. Verhoye, J.V. Audekerke, J. Sijbers, Maximum likelihood estimation-based denoising of magnetic resonance images using restricted local neighborhoods, Phys. Med. Biol. 56 (August (16)) (2011) 5221–5234.
[20] J. Rajan, J.D. Decker, J. Juntu, J. Sijbers, A new non-local maximum likelihood estimation method for Rician noise reduction in magnetic resonance images using the Kolmogorov–Smirnov test, Signal Process. 103 (2014) 19–23.
[21] J. Rajan, J.V. Audekerke, A.V. Linden, M. Verhoye, J. Sijbers, An adaptive non local maximum likelihood estimation method for denoising magnetic resonance images, IEEE Intern. Symp. Biomed. Imaging (2012, May) 1136–1139.
[22] P. Bao, L. Zhang, Noise reduction for magnetic resonance images via adaptive multiscale products thresholding, IEEE Trans. Med. Imaging 22 (September (9)) (2003) 1089–1099.
[23] D.D. Muresan, T.W. Parks, Adaptive principal components and image denoising, in: IEEE Intern. Conf. Image Process., vol. 1, 2003, pp. 101–104.
[24] L.P. Yaroslavsky, K. Egiazarian, J. Astola, Transform domain image restoration methods: review, comparison and interpretation, in: Proc. SPIE Intern. Conf. Nonlinear Image Proc. and Pattern Anal., vol. 4304, 2001, pp. 155–169.
[25] J. Sijbers, A.J. Dekker, P. Scheunders, D. Van Dyck, Maximum-likelihood estimation of Rician distribution parameters, IEEE Trans. Med. Imaging 17 (June (3)) (1998) 357–361.
[26] J. Sijbers, D.H.J. Poot, A.J. Dekker, W. Pintjens, Automatic estimation of the noise variance from the histogram of a magnetic resonance image, Phys. Med. Biol. 52 (February (5)) (2007) 1335–1348.
[27] J. Sijbers, A.J. Dekker, Maximum likelihood estimation of signal amplitude and noise variance from MR data, Magn. Reson. Med. 51 (March (3)) (2004) 586–594.
[28] L. Jiang, W. Yang, Adaptive magnetic resonance imaging denoting using mixture model and wavelet shrinkage, in: Proc. Int. Conf. on Digit. Imag. Comput.: Techniques and Applications, 2003, December.
[29] P. Fillard, V. Arsigny, X. Pennec, N. Ayache, Clinical DT-MRI estimation, smoothing and fiber tracking with log-Euclidean metrics, IEEE Trans. Med. Imaging 26 (November (11)) (2007) 1472–1482.
[30] A. Wong, A.K. Mishra, Quasi-Monte Carlo estimation approach for denoising MRI data based on regional statistics, IEEE Trans. Biomed. Eng. 58 (April (4)) (2011) 1076–1083.
[31] S. Aja-Fernández, C. Alberola-Lopez, C.F. Westin, Noise and signal estimation in magnitude MRI and Rician distributed images: a LMMSE approach, IEEE Trans. Imaging Process. 17 (August (8)) (2008) 1383–1398.
[32] S. Aja-Fernandez, M. Niethammer, M. Kubicki, M.E. Shenton, C.F. Westin, Restoration of DWI data using a Rician LMMSE estimator, IEEE Trans. Med. Imaging 27 (October (10)) (2008) 1389–1403.
[33] P.V. Sudeep, P. Palanisamy, J. Rajan, A hybrid model for Rician noise reduction in MRI, in: Proc. Int. Conf. Advanced Computing, Networking and Security (ADCONS), 2013, December, pp. 56–61, http://dx.doi.org/10.1109/ADCONS.2013.29
[34] H.M. Golshan, R.P.R. Hasanzadeh, C. Shahrokh Yousefzadeh, An MRI denoising method using image data redundancy and local SNR estimation, Magn. Reson. Imaging 31 (September (7)) (2013) 1206–1217.
[35] J. Mohan, V. Krishnaveni, Y. Guo, MRI denoising using nonlocal neutrosophic set approach of Wiener filtering, Biomed. Signal Process. Control 8 (November (6)) (2013) 779–791.
[36] G. Tian-li, L. Qie-gen, L. Jian-hua, Filter bank based nonlocal means for denoising magnetic resonance images, Springer J. Shanghai Jiaotong University (Science) 19 (April (1)) (2014) 72–78.
[37] R. Riji, J. Rajan, J. Sijbers, Madhu SN, Iterative bilateral filter for Rician noise reduction in MR images, Springer J. Signal Image Video Process. (2014, January) 1663–1703, http://dx.doi.org/10.1007/s11760-013-0611-6
[38] G. Perez, A. Conci, A.B. Moreno, J.A. Hernandez-Tamemes, Rician noise attenuation in the wavelet packet transformed domain for brain MRI, J. Integr. Comput-Aided Eng. 21 (April (2)) (2014) 163–175.
[39] A.J. Dekker, J. Sijbers, Data distributions in magnetic resonance images: a review, Phys. Med. 30 (November (7)) (2014) 725–741.
[40] R.M. Henkelman, Measurement of signal intensities in the presence of noise in MR images, Med. Phys. 12 (1985) 232–233.
[41] J. Sijbers, A.J. Dekker, M. Verhoye, J. Van Audekerke, D. Van Dyck, Estimation of noise from magnitude MR images, Magn. Reson. Imaging 16 (December (1)) (1998) 87–90.
[42] S. Aja-Fernandez, A.T. Vega, C.A. López, Noise estimation in single- and multiple-coil magnetic resonance data based on statistical models, Magn. Reson. Imaging 27 (December (10)) (2009) 1397–1409.
[43] P. Coupé, J.V. Manjón, E. Gedamu, D. Arnold, M. Robles, D.L. Collins, Robust Rician noise estimation for MR images, Med. Image Anal. 14 (August (4)) (2010) 483–493.
[44] J. Rajan, D. Poot, J. Juntu, J. Sijbers, Noise measurement from magnitude MRI using local estimates of variance and skewness, Phys. Med. Biol. 55 (August) (2010) N441–N449.
[45] A. Cichocki, S. Amari, Principal/Minor Component Analysis and Related Problems, in: Adapt. Blind Sign. and Image Process.: Learn. Algo. and Appl., 1st ed., J. Wiley, New York, 2005, pp. 87–125.
[46] L. Zhang, W. Dong, D. Zhang, G. Shi, Two-stage image denoising by principal component analysis with local pixel grouping, Pattern Recognit. 43 (April (4)) (2010) 1531–1549.
[47] J. Hu, Y. Pu, X. Wu, Yi Zhang, J. Zhou, Improved DCT-based nonlocal means filter for MR images denoising, Comput. Math. Meth. Med. 2012 (2012), http://dx.doi.org/10.1155/2012/232685
[48] Anon, https.//sites.google.com/site/myronenko/software /mirt_dctn.m.
[49] Anon, http://www.bic.mni.mcgill.ca/brainweb
[50] A. Buades, B. Coll, J.M. Morel, A nonlocal algorithm for image denoising, in: Proc. IEEE Computer Society Conf. Comp. Vision and Pattern Recognit. (CVPR), vol. 2, 2005, June, pp. 20–25.
[51] Y. Fisher, Fractal Image Compression: Theory and Application, 1st ed., Springer, London, UK, 1995.
[52] Z. Wang, A.C. Bovik, H.R. Sheik, E.P. Simoncelli, Image quality assessment: from error visibility to structural similarity, IEEE Trans. Imaging Process. 13 (April (4)) (2004) 600–612.
[53] A. Bhattacharyaa, On the measure of divergence between two statistical populations defined by their probability distributions, Bull. Calcutta Math. Soc. 35 (1) (1943) 99–109.